

THE EXTERNAL BEAM OF THE BERKELEY
184-INCH SYNCHROCYCLOTRON

Arthur C. Paul

November 24, 1971

AEC Contract No. W-7405-eng-48



For Reference
Not to be taken from this room

Printed in the United States of America
Available from
National Technical Information Service
U.S. Department of Commerce
5285 Port Royal Road
Springfield, Virginia 22151
Price: Printed Copy \$3.00; Microfiche \$0.95

DISCLAIMER

This document was prepared as an account of work sponsored by the United States Government. While this document is believed to contain correct information, neither the United States Government nor any agency thereof, nor the Regents of the University of California, nor any of their employees, makes any warranty, express or implied, or assumes any legal responsibility for the accuracy, completeness, or usefulness of any information, apparatus, product, or process disclosed, or represents that its use would not infringe privately owned rights. Reference herein to any specific commercial product, process, or service by its trade name, trademark, manufacturer, or otherwise, does not necessarily constitute or imply its endorsement, recommendation, or favoring by the United States Government or any agency thereof, or the Regents of the University of California. The views and opinions of authors expressed herein do not necessarily state or reflect those of the United States Government or any agency thereof or the Regents of the University of California.

THE EXTERNAL BEAM OF THE
BERKELEY 184-INCH SYNCHROCYCLOTRON

Arthur C. Paul

Lawrence Berkeley Laboratory
University of California
Berkeley, California 94720

November 24, 1971

ABSTRACT

The experimentally determined external beam properties of the main beam and satellite beam of the Berkeley 184-inch synchrocyclotron are discussed and compared to a computer model based on elliptical phase space contours. Reasonable agreement is found for the profile of both beams and the relative centroid positions. The starting conditions of the beams are tabulated at several useful locations along the beam line. Comparison is also made to the phase space contours calculated from an extraction study based on the cyclotron's magnetic field and betatron oscillation amplitudes.

1. Introduction

Figure 1 shows the extraction system of the 184 inch synchro-cyclotron and the external beam components leading up to the physics cave snout. Beam measurements have been performed at the 105 deg probe line, the premagnet collimator and at the physics cave snout. These measurements have been used to deduce the radial and vertical phase space at the cyclotron probe line required to fit all the data, Fig. 2. An energy difference of 1.4 MeV between the main and satellite beams has been neglected in the calculations. Analysis of the data leads to the following conclusions: The beam at the probe line consists of two beams of approximately equal intensity separated by $3/4$ in. and radially converging together at 11 mrad. The inward beam (called the main beam) is at a strong vertical focus with a size of 0.1 in. This beam has a radial extent of 0.5 inches at the probe line with a radial waist further downstream and an energy of 747 MeV. The outer beam (called the satellite) has a vertical extent of 0.4 in. and a radial extent of 0.3 in. at the probe line and converges towards a waist in each phase plane. The phase space occupied by these beams, Fig. 2, neglect the tails and fins of the characteristic "fish" appearance of the beam, Fig. 3, and represent best fits to all of the available data described in this report.

2. Beam Measurements at the Probe Line

A set of three different measurements, taken at the 105 deg probe line of the cyclotron, is necessary to deduce the main and satellite beam size and separation there. The emergence of each beam and the angular deviation between them is found from measurements taken

downstream. These three measurements are: 1) radioautograph of the beam, showing its vertical size, 2) total activity scan of the foil, used in making the radioautograph to find the radial size of the beams, and 3) finger probe interception measurement with a TV camera downstream to deduce the radial separation of the main and satellite beams. The results of these measurements are shown in Figs. 3, 4, and 5.

Figure 4 shows the physics cave ion chamber reading and the foil activity as a function of radius. The necessity of dividing the beam into two components is apparent from Fig. 3, taken 120 inches beyond the snout, where the two beams are clearly separated. It is customary to call the beam of larger radius at the probe line the satellite beam. A reasonable decomposition of the two beams in the horizontal plane is made by choosing the satellite beam as $5/8$ in. FWHM and the main beam as $7/8$ in. FWHM, $3/4$ in. further in than the satellite beam. The beam separation at the premagnet collimator yields a relative angular convergence of the beams of 11 milliradians. The vertical size of the beam at the probe line is determined from the radioautograph shown in Fig. 3.

Figure 5 shows a schematic representation of the beam location and radial size for the last three revolutions, as determined by a finger probe. The probe head consisted of a copper block 2 in. azimuthally, 2 in. high, and $1/2$ in. wide (in the radial direction). This head was supported 8 inches beyond the end of the probe so as not to intercept the beam in the 8 inch window so created. The beam passing by the probe was monitored on a TV camera located 120 in. beyond the physics cave snout. Figure 5 shows the radii where the probe just begins to

intercept the various beams, and also where the probe blocks out the beam as much as possible. From the relative extent of the satellite and main beams on the last turn and on the next to last turn, we conclude that the satellite beam can be removed with a 1/2 in. wide absorber of sufficient thickness placed at a radius of 91 inches; the main beam can be removed with the probe at either 86.50 or 90.20 inches. Both beams have a vertical focus at the probe line.

3. Premagnet Collimator Measurements

The premagnet collimator slits were adjusted for a small horizontal opening (4 div \approx 1/4 inch) and full opening vertically. A sweep across the beam was then made, measuring the physics cave ion chamber current as a function of the slit center position. These horizontal sweeps are shown in Figure 6. Three separate sweeps were made, one with the main beam blocked by the probe at 86.5 inches, one with the satellite beam blocked at 91.0 inches, and one with no probe, so that both beams were present. These sweeps confirm measurements made three years earlier. It should be noted that if the main beam and satellite beam sweeps are added, the result is very close to the sweep with both beams present. Both beams appear to be 2.3 in. FWHM and separated by 1.3 inches. Vertically, the sweeps were made by centering the slits on the beam and then opening the slit separation to maximum. It was found that the current was proportional to the slit opening out to a maximum opening of 6 inches.

4. Range Energy Measurements

A range energy measurement, Fig. 7, was performed on the primary proton beam in the physics cave to ascertain if an energy

difference exists between the main and satellite beams. The undesired beam was blocked by the main probe while the range of the other beam was determined. A range difference between the main and satellite beams was measured to be 0.037 in. of copper, corresponding to a 1.4 MeV energy difference — or a momentum difference of -0.12% for the satellite beam, relative to the main beam. The main beam range of 13.660 in. copper corresponds to an energy of 747.5 MeV. This is slightly higher than the maximum energy used in the computer extraction studies,¹⁾ [due to a magnetic field calibration error in the data used in the computer calculations²⁾].

The range measurement was performed with all apertures fully open. However, the satellite beam hit the physics cave quadrupole, as will be shown later, and the scattering so produced probably led to a slight shift in the center of gravity of the range measurement and consequently to the 1.4 MeV energy difference. However, this energy difference was sufficiently small so that it could be neglected in the subsequent calculations.

6. Beam Measurement at Several Quad Settings

The beam sizes and separation were measured by exposing polaroid film at the physics cave snout and 120 in. beyond it. These photographs are shown in Figure 3, 10-15. The tilt and angular projection of the phase ellipses of both beams in each phase plane were adjusted to give the best fit to the beam photos taken at the various quadrupole settings. Some of the beam pictures (notably Figs. 7 and 8) did not adequately represent two separate beams of given horizontal and vertical extent. In this case, only the size of the total beam, taken collectively, was

used. The physics cave quadrupole shunt readings were related to the field values at the pole tip by the calibration figure of 192 gauss/millivolt. Table 1 shows the beam half-sizes and centroid displacements in inches, at the physics cave snout and 120 in. beyond it (at the exit to CERCES).

7. Fitting the Beam Line With TRANSPORT

The convergence of the main beam and satellite beam centroids at the probe line, and the physics cave quadrupole alignment were treated as variables. These were adjusted to fit the centroid data of 0.75 in. at the probe, 1.3 in. at the premagnet collimator, and -1.0 in. at the physics cave snout, for quadrupole settings of -4.75 and 5.70 kG. The solution obtained indicated a convergence of 11 mrad at the probe line and a quadrupole misalignment of $X = -1.0$ in. for the satellite beam. There was no centroid divergence or quadrupole misalignment for the main beam. The calculations were carried out by a computer code, TRANSPORT,⁴⁾ as described in Section 9.

8. Cyclotron Fringe Field Matrix

The effect of the cyclotron magnetic channel and fringing field on the beam is expressed by a matrix, calculated for the standard magnetic field of the 184-inch cyclotron. This field has already been reported.^{1,2} The beam is considered to start at the 105 deg main probe line of the cyclotron, Fig. 1, and passes through the magnetic channel out into the rapidly decreasing fringe field of the cyclotron. The fringe field reverses sign at ~ 125 in. radius and is assumed to end at this point. The matrix transforming the beam from the probe line to the 125 in. radius was calculated by the computer code TRAJ³⁾ and is given below. The pariaxial ray for this matrix starts at a radius of 90.024 in. and 105 deg

azimuth, with an outward angle of 3.732 deg at 725.536 MeV. The orbit ends at 125 in. and 183.35 deg azimuth, with an outward angle of 35.36 degrees.

$$m = \begin{pmatrix} 3.5389 & .15815 & 0 & 0 & +.78573 \\ 29.779 & 1.61335 & 0 & 0 & +10.7707 \\ 0 & 0 & -2.19687 & .09392 & 0 \\ 0 & 0 & -13.9892 & .14285 & 0 \\ 0 & 0 & 0 & 0 & 1 \end{pmatrix}$$

The vector space upon which this matrix acts is X, X', Y, Y', $\delta P/P$ in units of inches, milliradians, inches, milliradians, and percent. The matrix to the premagnet collimator from the 105 degree probe line is

$$\begin{pmatrix} 5.2662 & .25172 & 0 & 0 & 1.4104 \\ 29.779 & 1.6133 & 0 & 0 & 10.771 \\ 0 & 0 & 3.0083 & .10221 & 0 \\ 0 & 0 & -13.989 & .14285 & 0 \\ 0 & 0 & 0 & 0 & 1 \end{pmatrix}$$

9. Transport Beamline Calculations

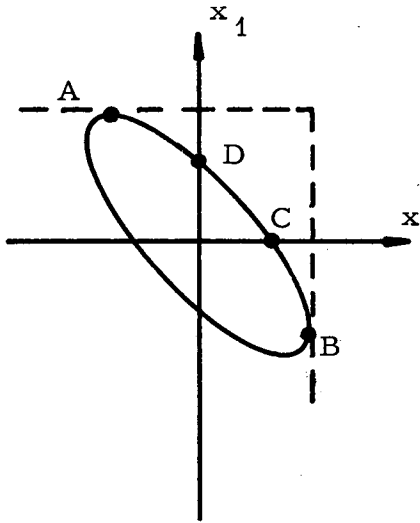
The physics cave external beam line was considered to start at the 105 deg probe line of the cyclotron and to pass through the magnetic channel, premagnet collimator, steering magnet, and physics cave quadrupole, ending at the physics cave snout, Fig. 1. The beam line was described by standard transport⁴⁾ data, as shown in Fig. 16. The beam angular divergence, centroid convergence, and the quadrupole alignment for the satellite beam were treated as variables to be fit to the observed beam profile data. The appropriate quadrupole field strength was used for each profile. The beam alignment calculation

acted only on the beam ellipsoid, as defined by the type 1 and 12 data entries, and did not affect the ellipsoids defined by the various particle vectors and type 22 data entries (see UCID-3525 for a full discussion of data types and usage). In this way, both the satellite and main beams could be tracked and displayed, under the assumption that the main beam was aligned and represented by vectors 2-11, while the satellite beam was represented by the beam ellipsoid and misaligned with respect to the quadrupole. Vectors 13 through 22 showed the satellite beam masking any centroid shift and overlay points on the beam ellipsoid.

After finding the optimal values of the angular divergence and quadrupole misalignment, computer runs were made at each of the quadrupole settings given in Table 1 and are shown in Figs. 17-23. The horizontal and vertical size of each beam and its relative horizontal centroid shift, as computed, is indicated for comparison to the observed values, listed in Table 1 and shown in Figs. 4, 10, 11, 12, 13, 14, and 15.

10. Finding Transport Beam Tilts From Measured Projections

If we know the measured projections, A and B, of the phase ellipse on both coordinate axes, the tilt of the phase ellipse can be determined by knowing the intersection point of the ellipse with either axes, C or D, as shown in the accompanying sketch.



The equation of the beam ellipse in matrix notation is:

$$(x \ x') \begin{pmatrix} S_{11} & S_{21} \\ S_{21} & S_{22} \end{pmatrix} \begin{pmatrix} x \\ x' \end{pmatrix} = 1$$

Expanding, we have:

$$S_{22}x^2 - 2S_{21}xx' + S_{11}x'^2 = S_{22}S_{11} - S_{21}^2$$

At point A, $dx'/dx = 0$; at point B, $dx/dx' = 0$; at point C, $x' = 0$; and at point D, $x = 0$

Solving this equation we find:

$$S_{11} = B^2;$$

$$S_{22} = A^2;$$

$$S_{21} = A(B^2 - C^2)^{1/2}.$$

In transport notation we define the normalized tilt as

$$r_{21} = \sqrt{\frac{S_{21}}{S_{22}S_{11}}}.$$

therefore:

$$r_{21} = \frac{1}{B} \sqrt{B^2 - C^2}.$$

11. Comparison With Extraction Study

A previous study of the extraction system of the 184-inch synchro-cyclotron¹⁾ predicted the radial and vertical phase space, based only on the magnetic field of the cyclotron and on the measured radial and vertical betatron oscillation amplitudes several hundred revolutions before extraction. The results of these calculations showed that

considerable nonlinearities were indeed encountered, as shown in Figs. 8 and 9. The "crossed ellipse" appearance of the vertical phase space, shown in Fig. 9, results from the presence of two beams of different vertical tune, and should be compared to Fig. 2, calculated from the backward transformation of external beam projections of the two beams. Figures 8 and 9 showing the beam at 105 in. radius, 166 deg azimuth, depict the radial and vertical phase space at the termination of the calculation, after extraction of particles which were started initially on elliptical phase space boundaries several hundred revolutions prior to extraction. Although the photographs at the snout, and also the orbit calculations, indicate a nonlinear character to the beam, we assume linearity in order to affect the mathematical simplicity of linear transformations. The approximated radial elliptical phase space boundaries and the corresponding nonlinear boundaries are shown in Fig. 8, and pertain to beams of 700, 715, and 730 MeV from a large sampling of vertical betatron amplitudes and vertical and horizontal phases. The largest vertical phase space that is used in this study corresponds to an initial vertical betatron oscillation amplitude of $1/8$ inch, prior to extraction, due to the large loss associated with larger betatron amplitudes.

In order to compare the idealized ellipsoids to those deduced from the measured beam profile, we transform the ellipses back to the probe line at 105 degrees. The required transformation matrix from 105 to 166 degrees is:

$$R = \begin{pmatrix} 2.621 & .1056 & 0 & 0 & .41716 \\ 12.916 & .90173 & 0 & 0 & 7.1741 \\ 0 & 0 & -1.4854 & .08073 & 0 \\ 0 & 0 & -24.502 & .65847 & 0 \\ 0 & 0 & 0 & 0 & 1 \end{pmatrix}$$

Its inverse is:

$$R^{-1} = \begin{pmatrix} .80173 & -.1056 & 0 & 0 & .38139 \\ 12.916 & 2.621 & 0 & 0 & -13.4193 \\ 0 & 0 & .6585 & -.08073 & 0 \\ 0 & 0 & 24.502 & -1.4854 & 0 \\ 0 & 0 & 0 & 0 & 1 \end{pmatrix}$$

The equivalent beam ellipsoid in transport notation at the pariaxial location of 106 in. radius, 166 deg azimuth is:

$$\begin{aligned} X &= 0.63 \text{ in.} & Y &= 2.20 \text{ in.} \\ X' &= 2.3 \text{ mrad} & Y' &= 27.2 \text{ mrad} \\ r_{21} &= 0.75 & r_{23} &= 0.9555 . \end{aligned}$$

When transformed to the cyclotron probe line, 90 in. radius, 105 deg azimuth, the equivalent beam ellipsoid becomes:

$$\begin{aligned} X &= 0.418 \text{ in.} & Y &= 0.829 \text{ in.} \\ X' &= 5.38 \text{ mrad} & Y' &= 12.7 \text{ mrad} \\ r_{21} &= -0.9047 & r_{43} &= -0.751 . \end{aligned}$$

These numbers can be given a little more meaning by noting that if we consider a field free transformation, the vertical beam approaches a waist 49 in. downstream and the radial beam a waist 70 in. downstream from the probe line.

Figure 3 shows that the vertical node must lie at the probe line for the last turn, and so the calculations must have a total error producing a 49 in. vertical node shift.

The satellite beam fit at the probe line shown in Fig. 2 is:

$$\begin{array}{ll} X = 0.3 \text{ in.} & Y = 0.4 \text{ in.} \\ X' = 6.0 \text{ mrad} & Y' = 16.0 \text{ mrad} \\ r_{21} = -0.90 & r_{43} = -.9 \end{array}$$

and compares reasonably well with the calculated value, except for the vertical beam size. The main beam fit shown in Fig. 2 is:

$$\begin{array}{ll} X = .5 \text{ in.} & Y = 0.1 \text{ in.} \\ X' = 6.0 \text{ mrad} & Y' = 10.0 \text{ mrad} \\ r_{21} = -.94 & r_{43} = 0 \end{array}$$

A beam of 715 MeV energy is -1% in $\delta p/p$ below the nominal energy of 730 MeV. The centroid for the 715 MeV beam is located at $\Delta Pr = -.016 \text{ cu}$ ⁵⁾ and $\Delta X = -.0018 \text{ cu}$ with respect to the 730 MeV beam, Fig. 8, at a beam location of 106 in. radius, 166 deg azimuth. Transforming back to the probe line we find the -1% vector as:

<u>105°, 90''</u>	<u>166°, 106''</u>
X (in.) = 0.529 ,	-.264
X' (mrad) = -11.7	-10.9
$\delta p/p(\%) = -1.0$	-1.0 .

The dispersion line formed by the 730 MeV beam and this 715 MeV beam is shown in Fig. 2.

⁵⁾ cu stands for cyclotron units and is discussed in Reference 1.

12. Conclusions

The beam phase space from the 184 inch cyclotron, for use in external beam calculations, should be that shown in Fig. 2, or with the beam appropriately transformed to some other location. The three most useful locations are those accessible to the experimentalist, namely the 105 deg probe line, the premagnet collimator, and the physics cave snout. The main and satellite beam ellipsoids in transport notation, and their relative centroid displacement, are tabulated in Table 2 at these three locations.

ACKNOWLEDGMENTS

Acknowledgment is given to Dr. Kenneth M. Crowe for many helpful discussions concerning the optic calculations, and to James Vale and the cyclotron crew, in particular to Leal Kanstein and James MacMullen, for taking most of the data reported here.

Work performed under the auspices of the U.S. Atomic Energy Commission.

REFERENCES

1. A. C. Paul, Study of the Regenerative Extractor of the Berkeley 184 inch Synchrocyclotron. (1968) UCRL-18211.
2. A. C. Paul, J. S. Colonias, Magnetic Field Calculation for the 184 inch Synchrocyclotron. (1970) UCRL-18882.
3. A. C. Paul, "TRAJECTORY" An Orbit and Ion Optic Matrix Program for the 184 inch Cyclotron. (1969) UCRL-19407.
4. A. C. Paul, UCRL Berkeley Version of TRANSPORT, (1971), UCID-3525.

TABLE 1

Beam sizes, as determined from the photographs taken at the physics cave snout and 120 inches beyond. The sizes are the displacements from the pariaxial ray, and as such, are half sizes. They are given as X × Y (Main beam)/X × Y (satellite beam), in inches. The first quadrupole is vertically focusing and the second is horizontally focusing. The field at the pole tip 4 in. off axis is given in kG.

Photo Figure	Vert. Lens Shunt (mV)	Horiz. Lens Shunt (mV)	Vert. Lens (kG)	Horiz. Lens (kG)	Snout		120" beyond snout		
					Beam Size (Inches)	+ Δ X Centroid (Inches)	Beam Size (Inches)	+ Δ X Centroid (Inches)	
1	--	--	--	--	--	--	--	--	
2	10	24.75	29.70	-4.752	5.7024	.6 × .3 / .5 × 2.	-.4 → -1.	.25 × .25 / .25 × 1.5	-2.0
3	3	26.87	29.92	-5.159	5.744	--	--	.5 × .5 / .3 × .3	-1.60
4	--	23.23	27.57	--	--	--	--	--	--
5	--	23.23	27.57	--	--	--	--	--	--
6	11	23.23	27.57	-4.460	5.293	1 × .5 / 1 × 2	-.5	.3 × .3 / .25 × 1.5	-1.75
7	12	26.58	27.57	-5.103	5.293	Both beams 2" Dense core .25" V.	?	1 × 1. / .8 × .5	-.30
8	13	23.23	24.91	-4.460	4.783	.5 × .125 spot HW 2 × 2" holo FW	?	3 × 1.5 FW	?
9	14	23.23	29.25	-4.460	5.616	.30-.5 × .5-1. / .5 × 2 ?	-.5 → -1.	.25 × .5 / .25 × 2	-2.0
10	15	28.25	31.47	-5.424	6.042	2" × 1" Both FW	-.5 → -1.5	.25 × 1 / .5 × .375	-1.5

000000/01/000

TABLE 2

Transport beam ellipses at three locations along the beam line for the beam phase space shown in Fig. 2

		105 degree probe line	Premagnet collimator	Physics cave snout Q1=-4.752 kG, Q2=5.7024 kG
main beam horizontal phase space	X(in.) X' (mrad) r_{21}	0.5(in.) 10.(mrad) -.94	.9(in.) 5.51(mrad) .939	.825(in.) 6.504(mrad) -.948
main beam vertical phase space	Y(in.) Y' (mrad) r_{43}	0.1(in.) 10.(mrad) 0.	1.065(in.) 2.0(mrad) .883	.423(in.) 2.457(mrad) -.337
satellite centroid shift	X(in.) X' (mrad) $\delta p/p$ (%)	0.75(in.) 11.0(mrad) 0.	1.181(in.) 4.587(mrad) 0.	-.403(in.) -14.705(mrad) 0.
satellite beam horizontal phase space	X(in.) X' (mrad) r_{21}	0.3(in.) 6.(mrad) -.9	.694(in.) .225(mrad) .964	.631(in.) 5.032(mrad) -.969
satellite beam vertical phase space	Y(in.) Y' (mrad) r_{43}	0.4(in.) 16.(mrad) -.9	2.768(in.) 7.717(mrad) .991	1.827(in.) 2.768(mrad) -.834
quadrupole misalignment	X(in.) X' (mrad)	-- --	-- --	-1.0(in.) 0(mrad)

TABLE 3

Input data for transport for main beam or satellite beam extending from probe line to the pre-magnet collimator.

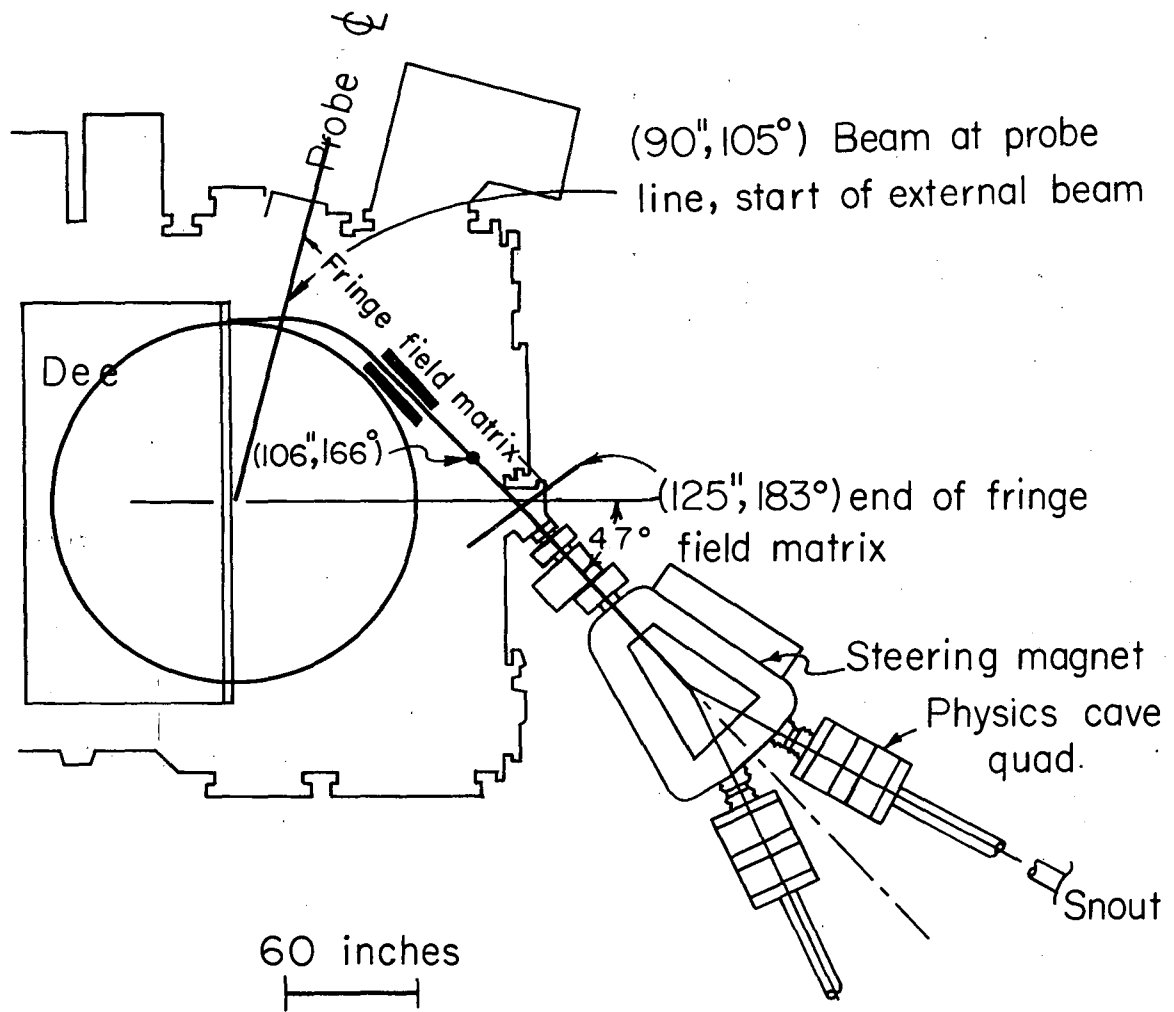
MAIN BEAM DATA TO PMC. SAT BEAM CENTROID VIA VECTOR FROM 105 DEG PROBE

0								
15.	2.	1.						
15.	1.	IN	2.54					
15.	8.	IN	0.0254					
22.	.75	-11.						
1.	.5	10.	.1	10.	0.	0.	1.3794	
12.	-.94	0.	0.	0.	0.	0.	0.	
0.	0.	0.	0.	0.	0.	0.	0.	
14.	3.539	.15815	0	0.	0.	0.78573	1.	
14.	29.7788	1.61335	0	0.	0.	10.77074	2.	
14.	0.	0.	-2.19687	.09392	0.	0.	3.	
14.	0.	0.	-13.9892	.14285	0.	0.	4.	
3.	58.							
73.								

SAT BEAM TO PMC FROM 105 DEG PROBE

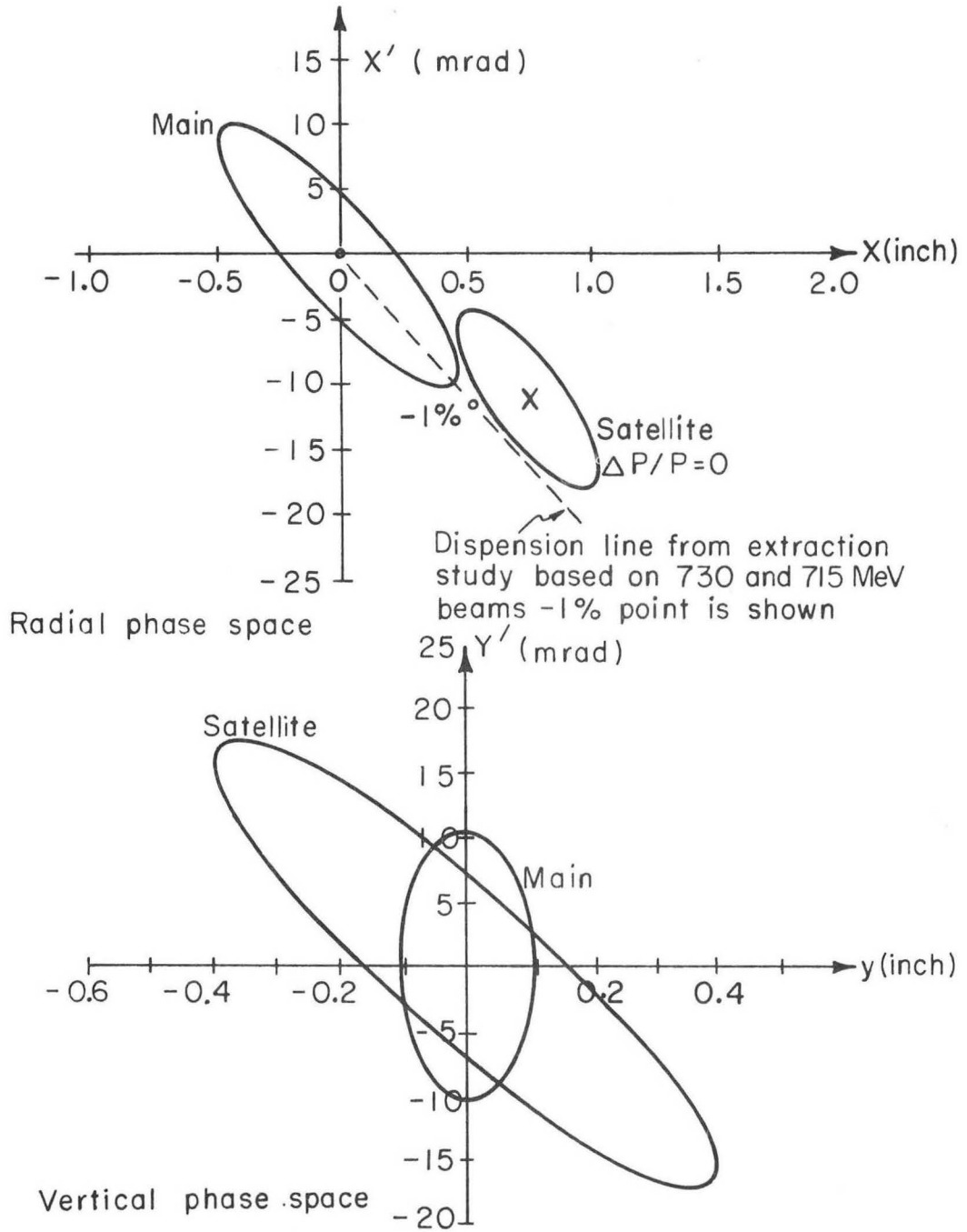
0								
15.	2.	1.						
15.	1.	IN	2.54					
15.	8.	IN	.0254					
22.								
1.	.3	6.	.4	16.	0.	0.	1.3794	
12.	-.9	0.	0.	0.	0.	-.9	0.	
0.	0.	0.	0.	0.	0.	0.	0.	
7.	.75	-11.						
14.	3.539	.15815	0.	0.	0.	.78573	1.	
14.	29.7788	1.61335	0.	0.	0.	10.77074	2.	
14.	0.	0.	-2.19687	.09392	0.	0.	3.	
14.	0.	0.	-13.9892	.14285	0.	0.	4.	
3.	58.							
73.								

0000070100



XBL722-2266

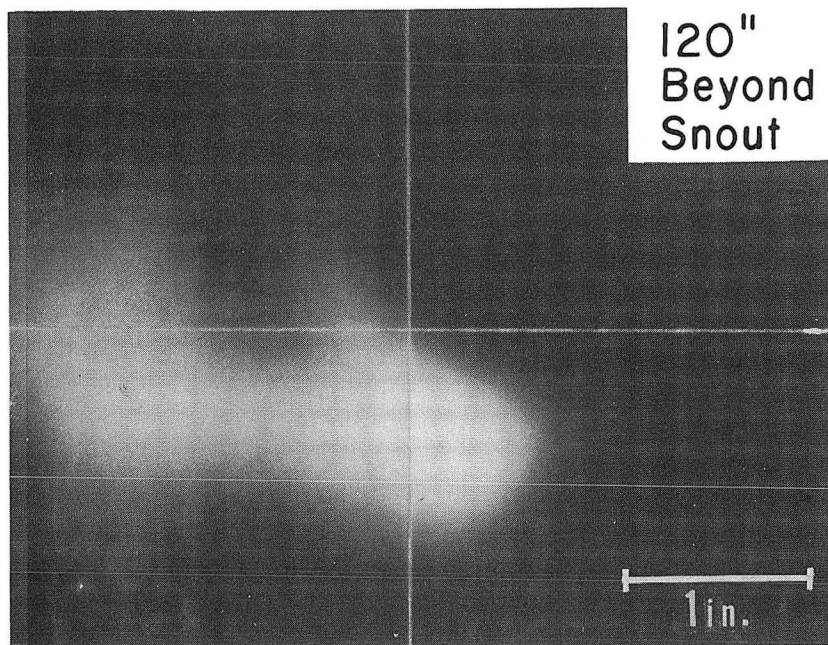
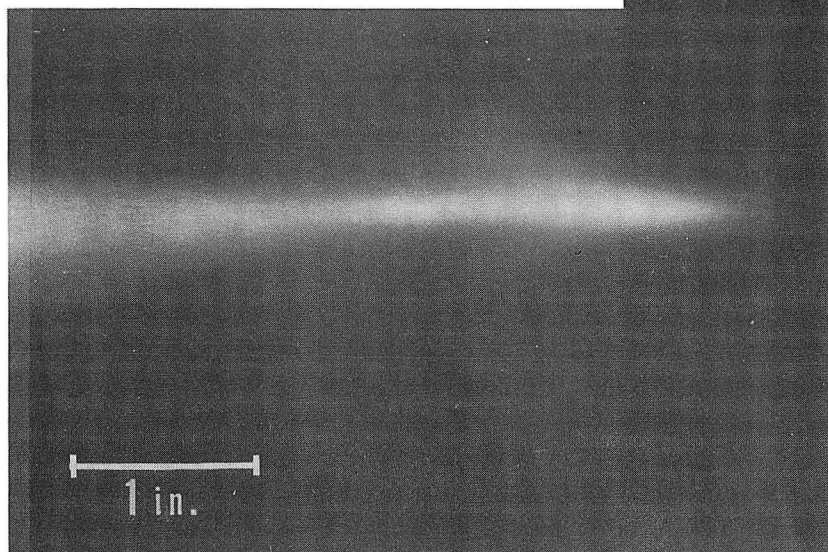
Fig. 1. Layout of the extraction system and external beam line of the 184-inch Synchrotron. XBL686-2951



XBL 722-2267

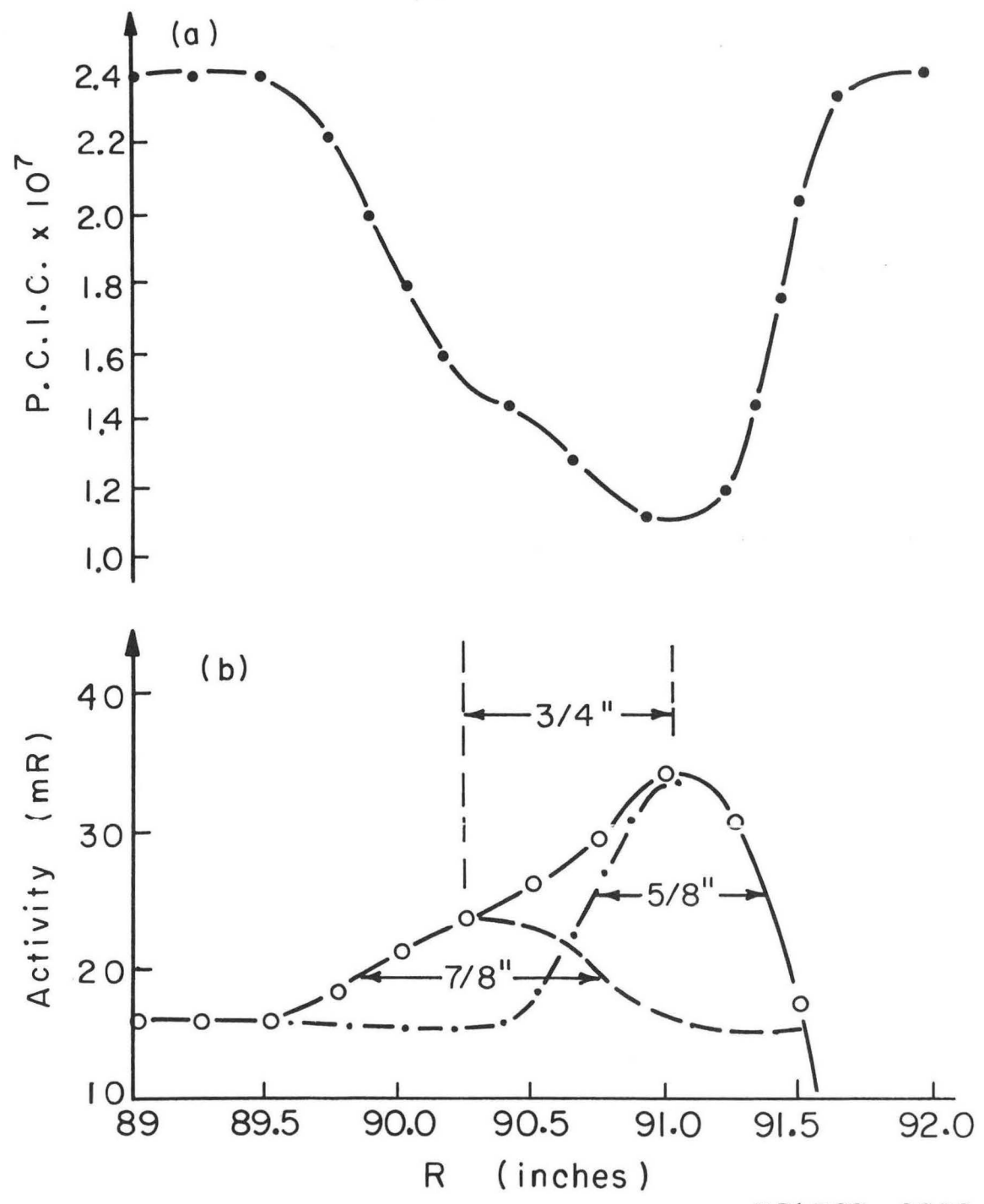
Fig. 2. Radial and vertical phase space at the 105 deg probe line, showing the main and satellite beams.

Radio-Autograph of Target
at 105 degree Probe



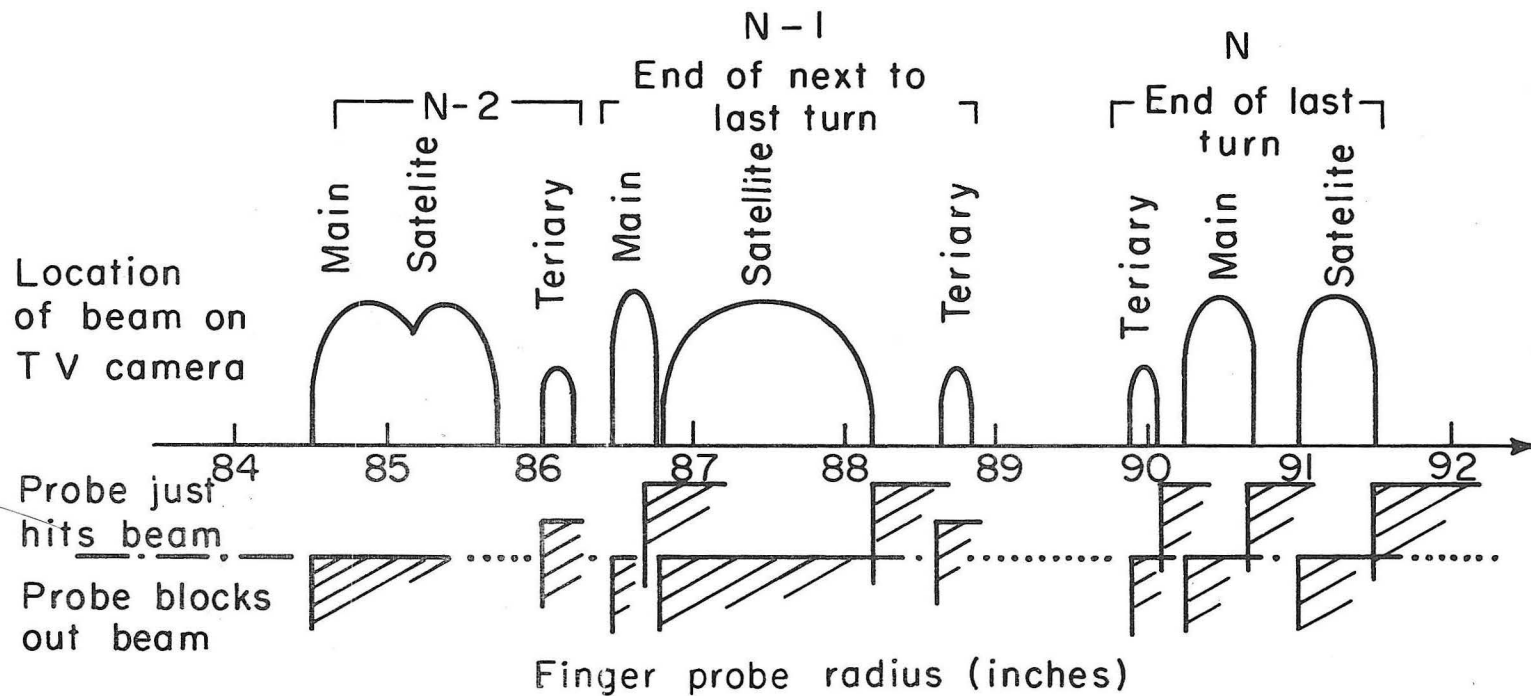
XBB 719-4601

Fig. 3. (a) Beam target radio-autograph, showing the beam prior to passage behind the magnetic regenerator. (b) The beam 120 inches beyond the physics cave snout, with the steering magnet set to 282.7 mV and the quadrupoles set to 26.87 mV and 29.92 mV.



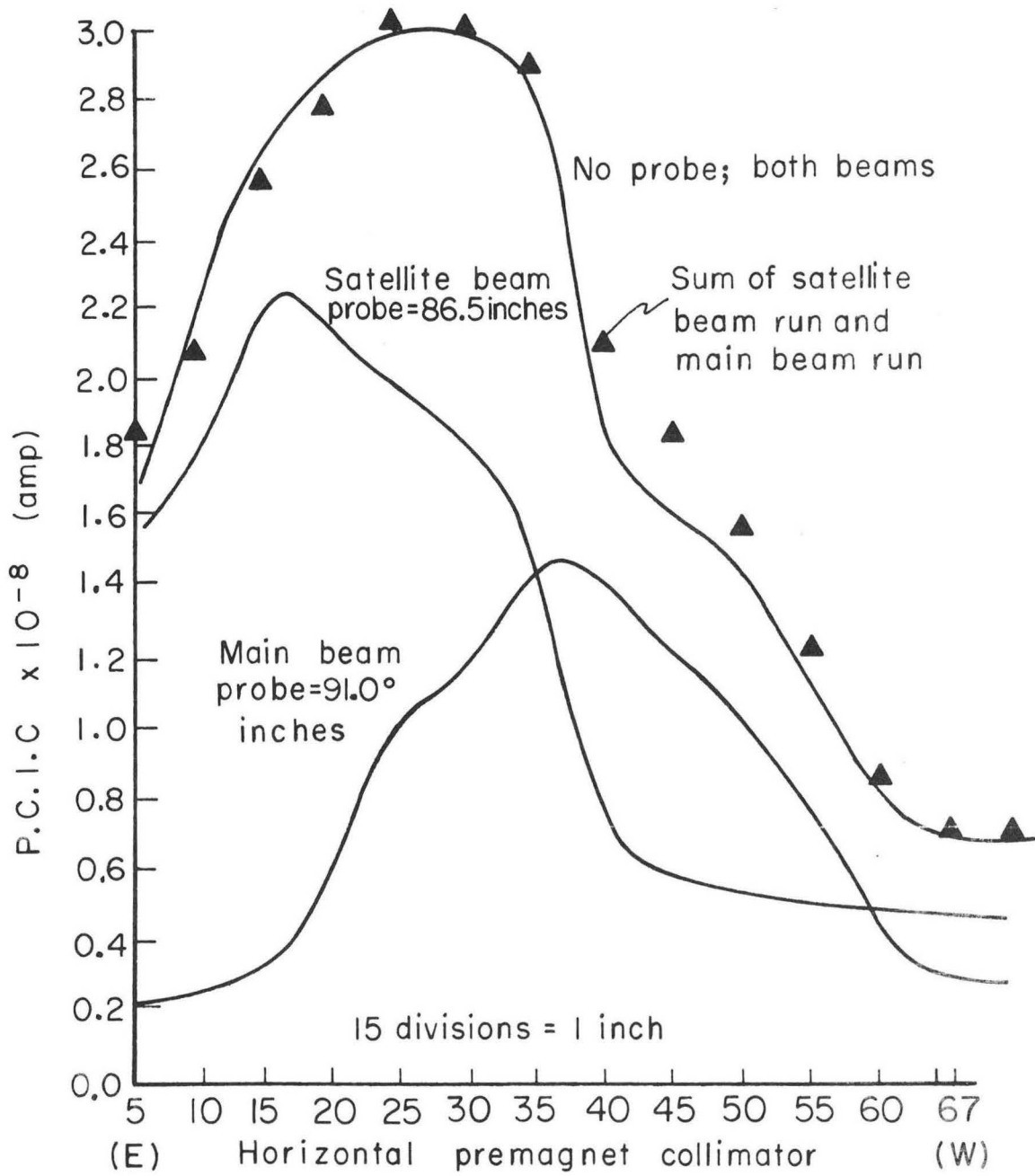
XBL722 - 2268

Fig. 4. (a) Physics cave ion chamber reading versus probe radius. (b) Activity of thin copper target versus position, showing decomposition into two beams.



XBL 722-2269

Fig. 5. Radial location of the extracted beams at the 105 degree probe line at the end of the last three turns.



XBL722-2270

Fig. 6. Horizontal premagnet collimator beam profiles as measured with the physics cave ion chamber.

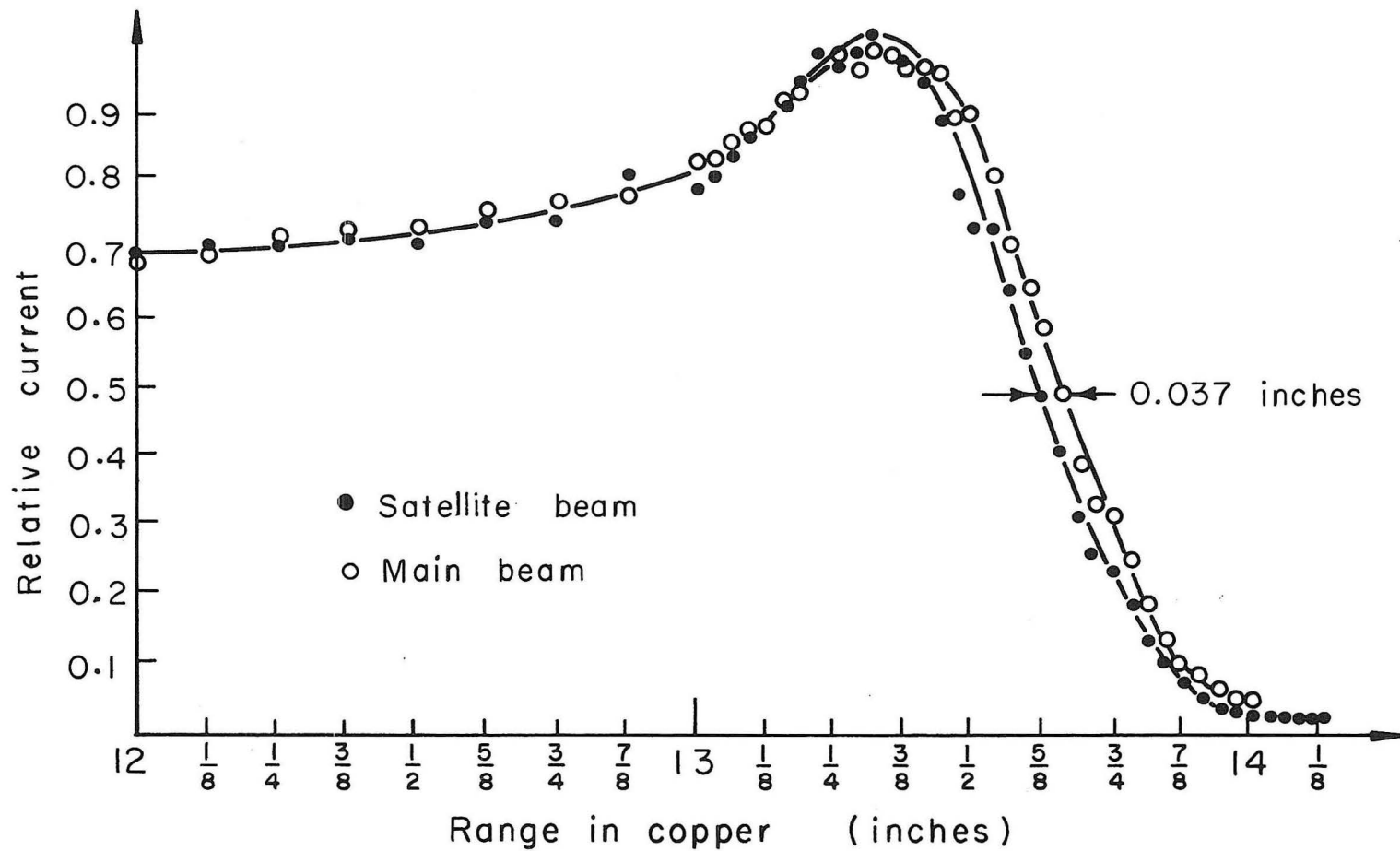


Fig. 7. Current vs. absorber thickness for main and satellite beams in the physics cave, normalized for equal area under curves from 12 to 13 3/8 inches. The range difference is 0.037 inches.

XBL722-2271

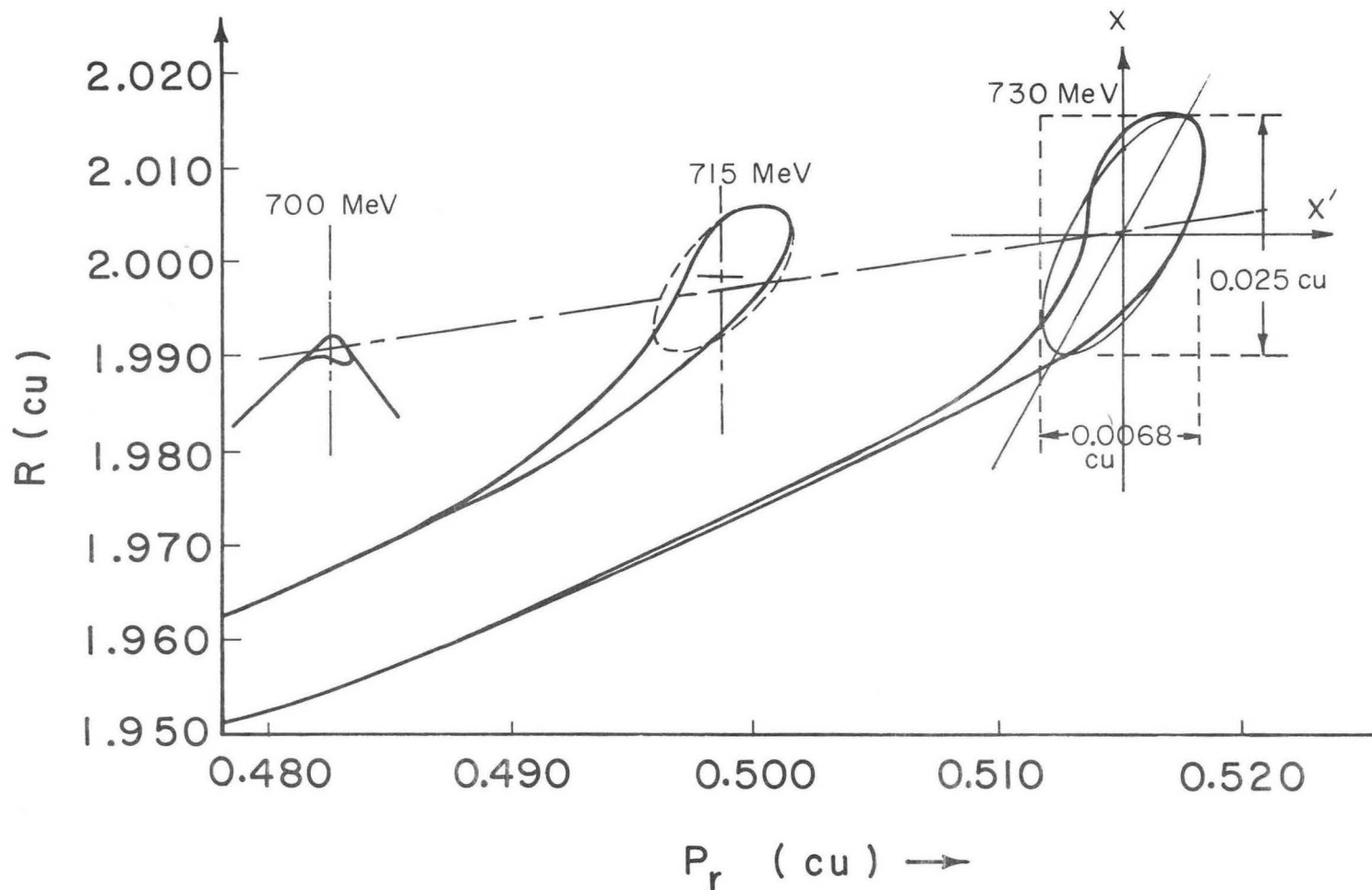
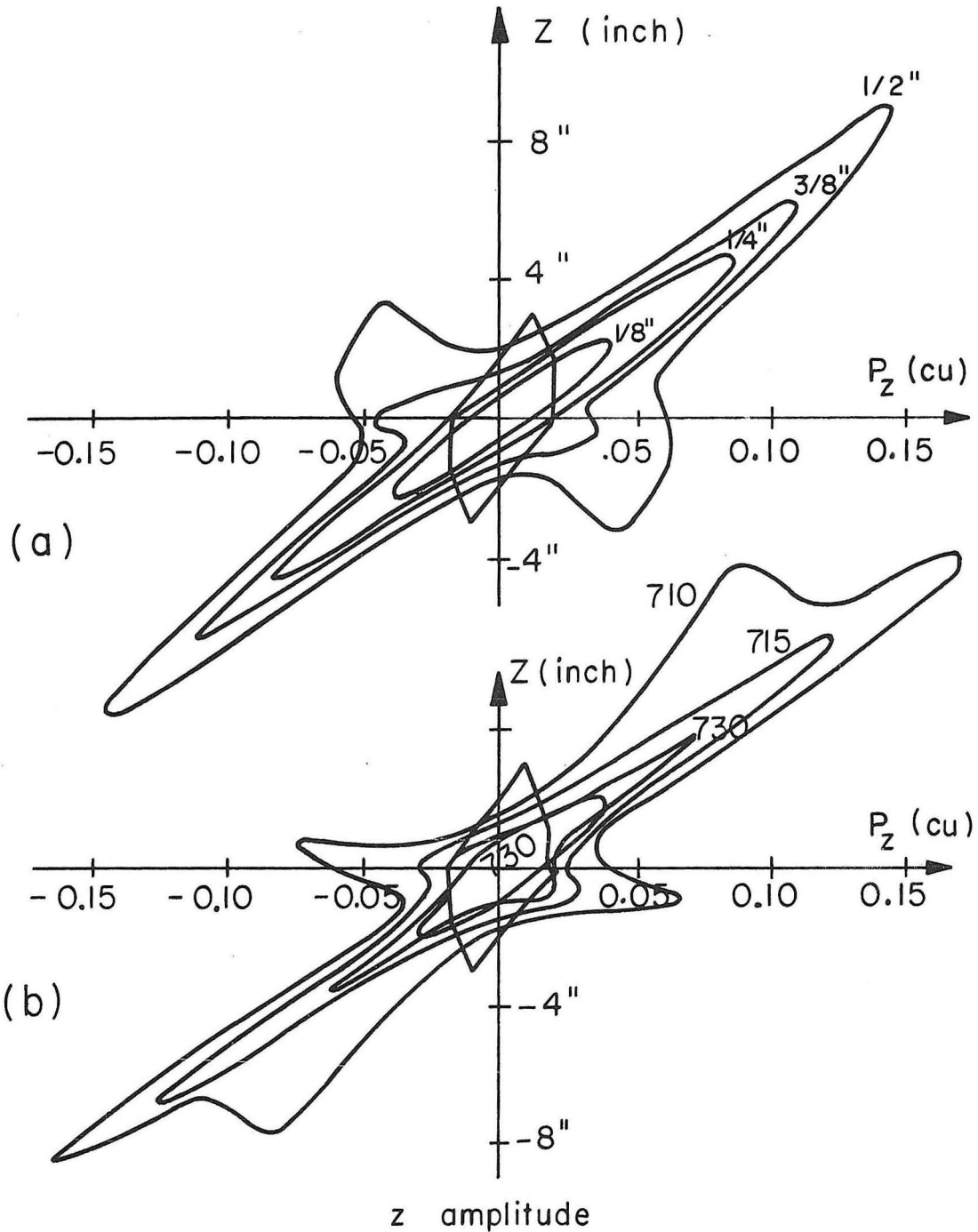


Fig. 8. Radial phase space at end of 184-inch cyclotron orbit study. Beam centroid at $R = 106$. $\theta = 166$ deg, UCRL-18211. One cyclotron unit (cu) is 52.767 inches. P_r is in units of MoC. The 730 MeV-equivalent ellipse in transport notation is $0.63\text{in} \times 2.3$ mrad with $r_{21} = 0.75$ ($p = 1.470$ cu).

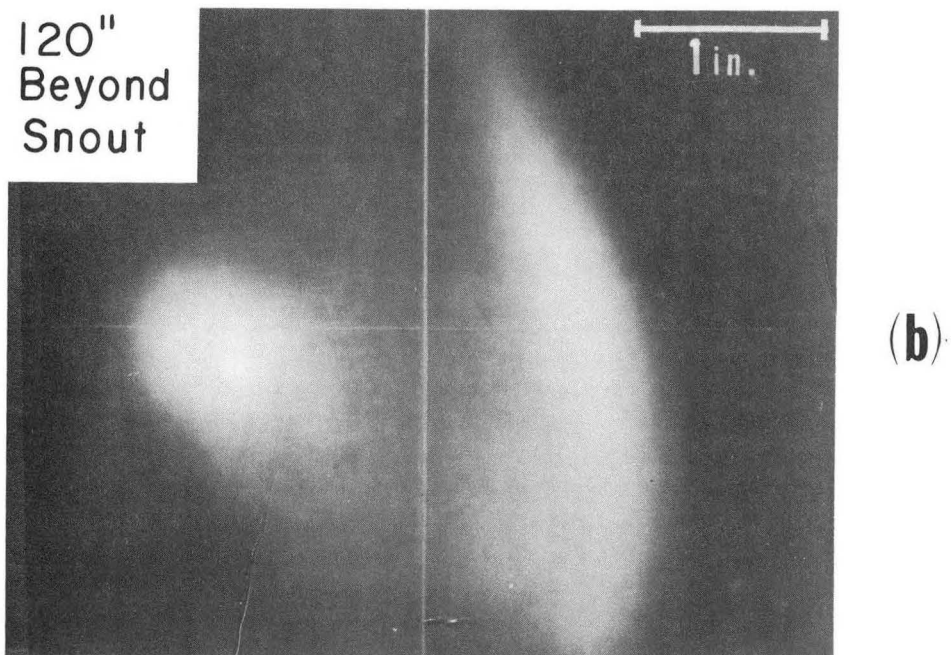
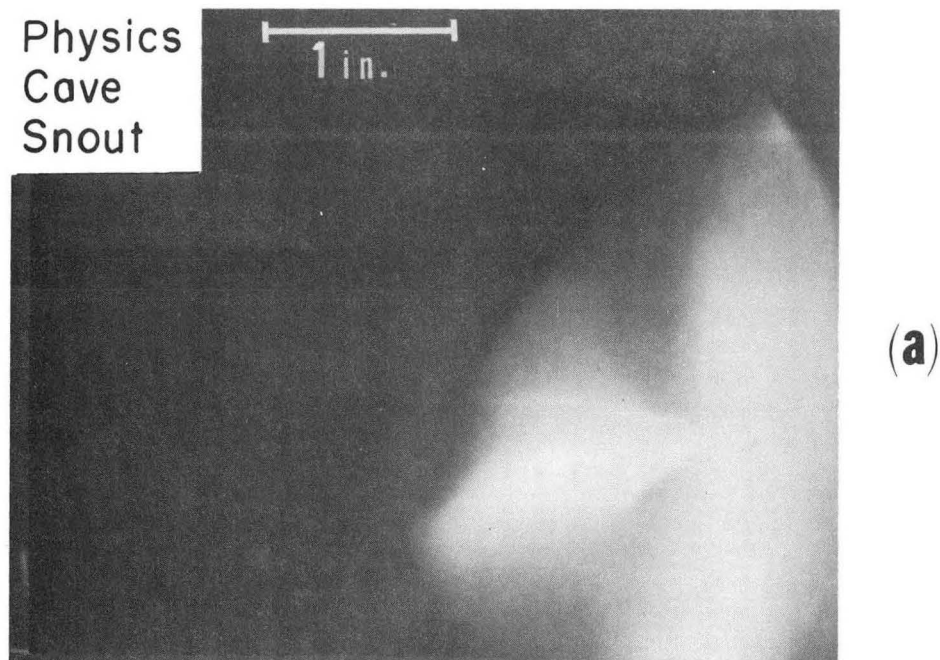
XBL 722-2272

00000701790



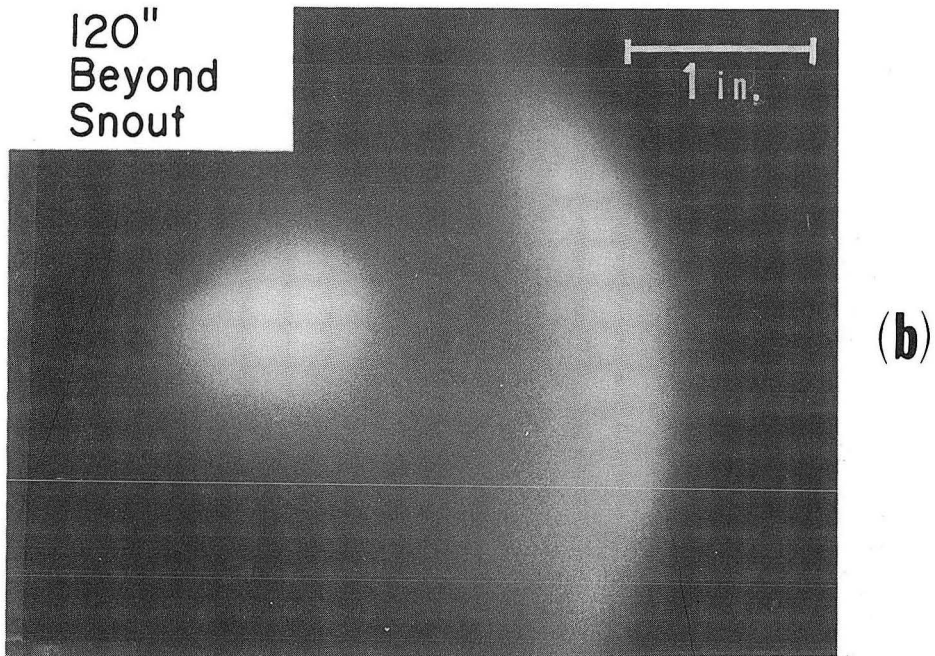
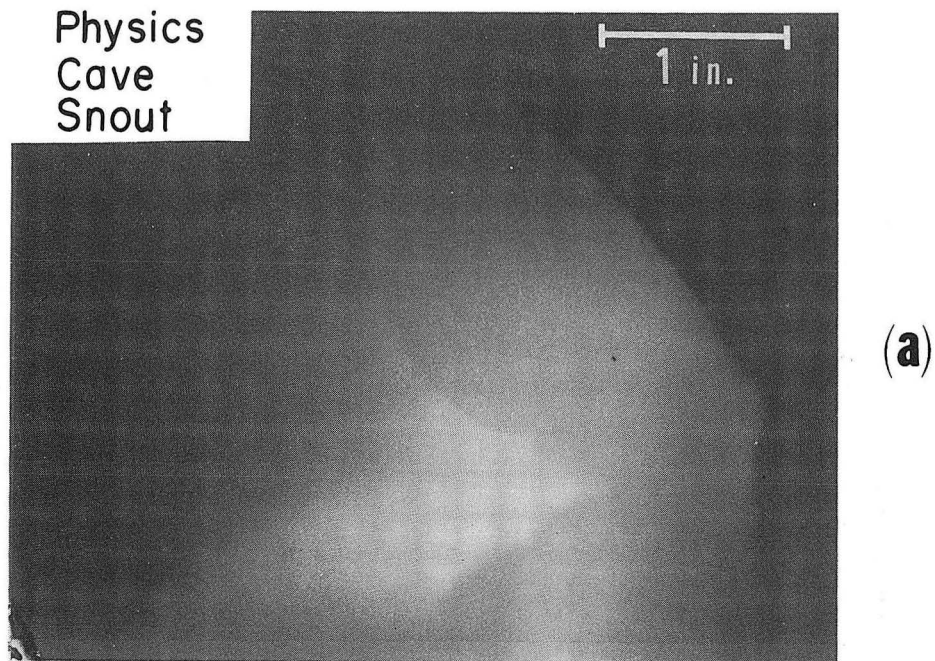
XBL722-2273

Fig. 9. Calculated 730 MeV vertical phase space at 106", 166° for z amplitude = 1/8, 1/4, 3/8, and 1/2 inches. Calculated 1/8 in. vertical phase space at 106", 166° for E = 730, 720, 715, and 710 MeV. No vertical or radial internal apertures.



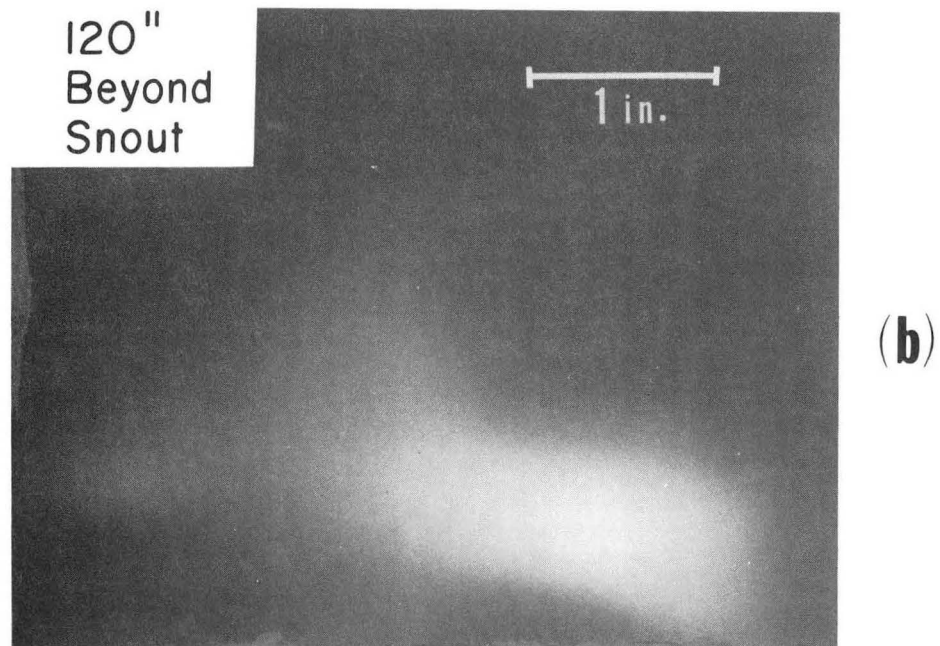
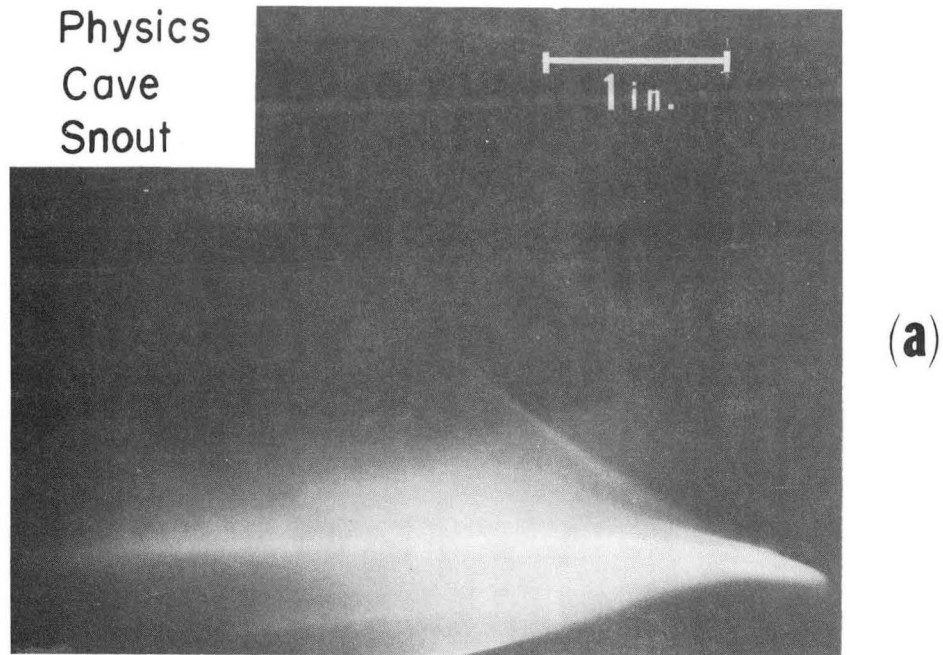
XBB 719-4603

Fig. 10. (a) Beam photograph #2 at physics cave snout. (b). Beam 120" beyond snout. Both photographs are viewed looking in the direction of beam travel, main beam on the left, satellite beam on the right. The steering magnet was set to 277.7 mV; quadrupoles were set to 24.75 mV and 29.70 mV.



XBB 719-4598

Fig. 11. (a) Beam photograph # 6 at physics cave snout.
(b) Beam 120" beyond snout. Both photographs are viewed looking in the direction of beam travel, main beam on the left, satellite beam on the right. The steering magnet was set to 281.5 mV; quadrupoles were set to 23.23 mV and 27.57 mV.



XBB 719-4602

Fig. 12. (a) Beam photograph #7 at physics cave snout. (b) Beam 120" beyond snout. Both photographs are viewed looking in the direction of beam travel, main beam on the left, satellite beam on the right. The steering magnet was set to 281.5 mV; quadrupoles were set to 26.58 mV and 27.57 mV.

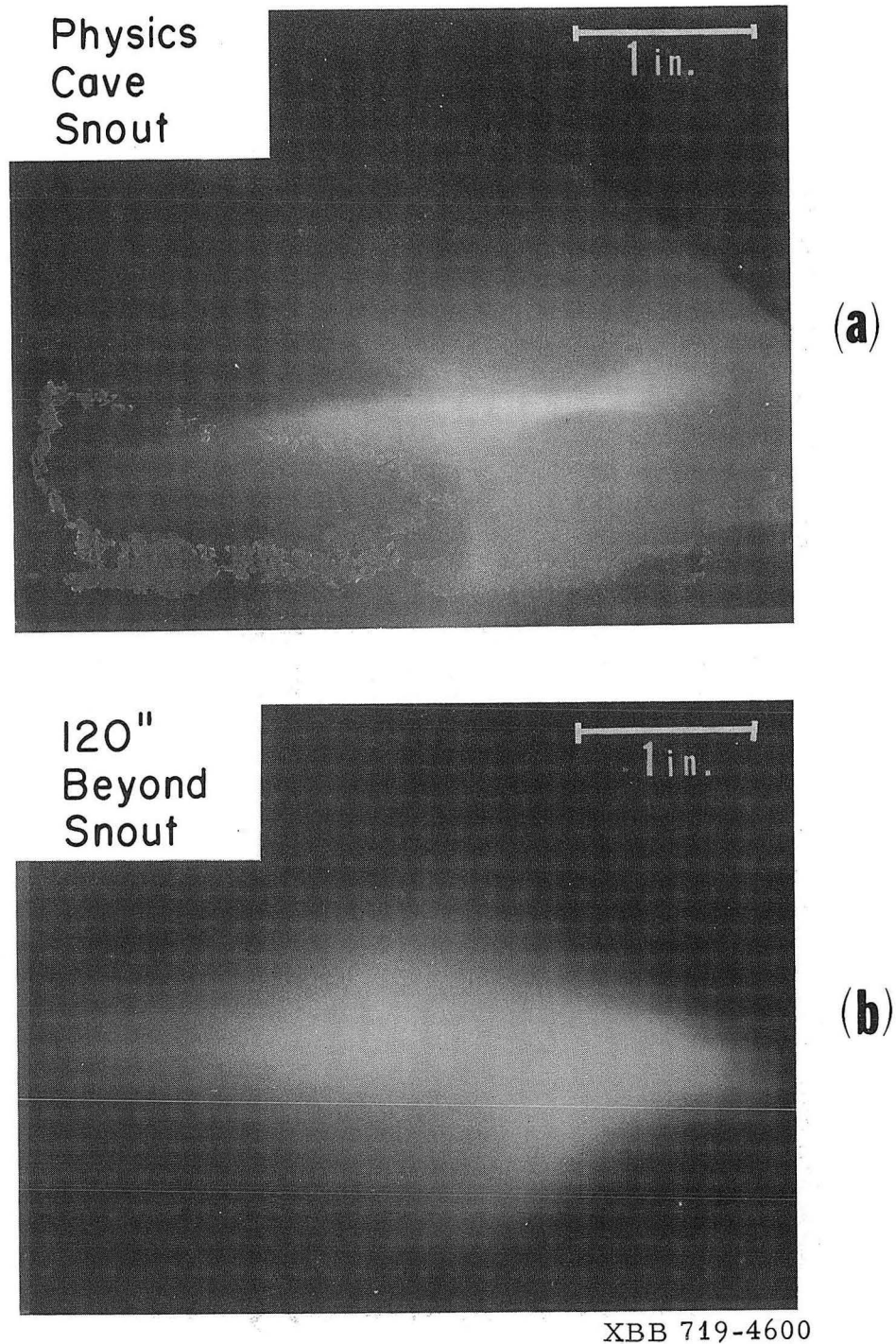


Fig. 13. (a) Beam photograph #8 at physics cave snout. (b) Beam 120" beyond snout. Both photographs are viewed looking in the direction of beam travel, main beam on the left, satellite beam on the right. The steering magnet was set to 281.5 mV; quadrupoles were set to 23.23 mV and 24.91 mV.

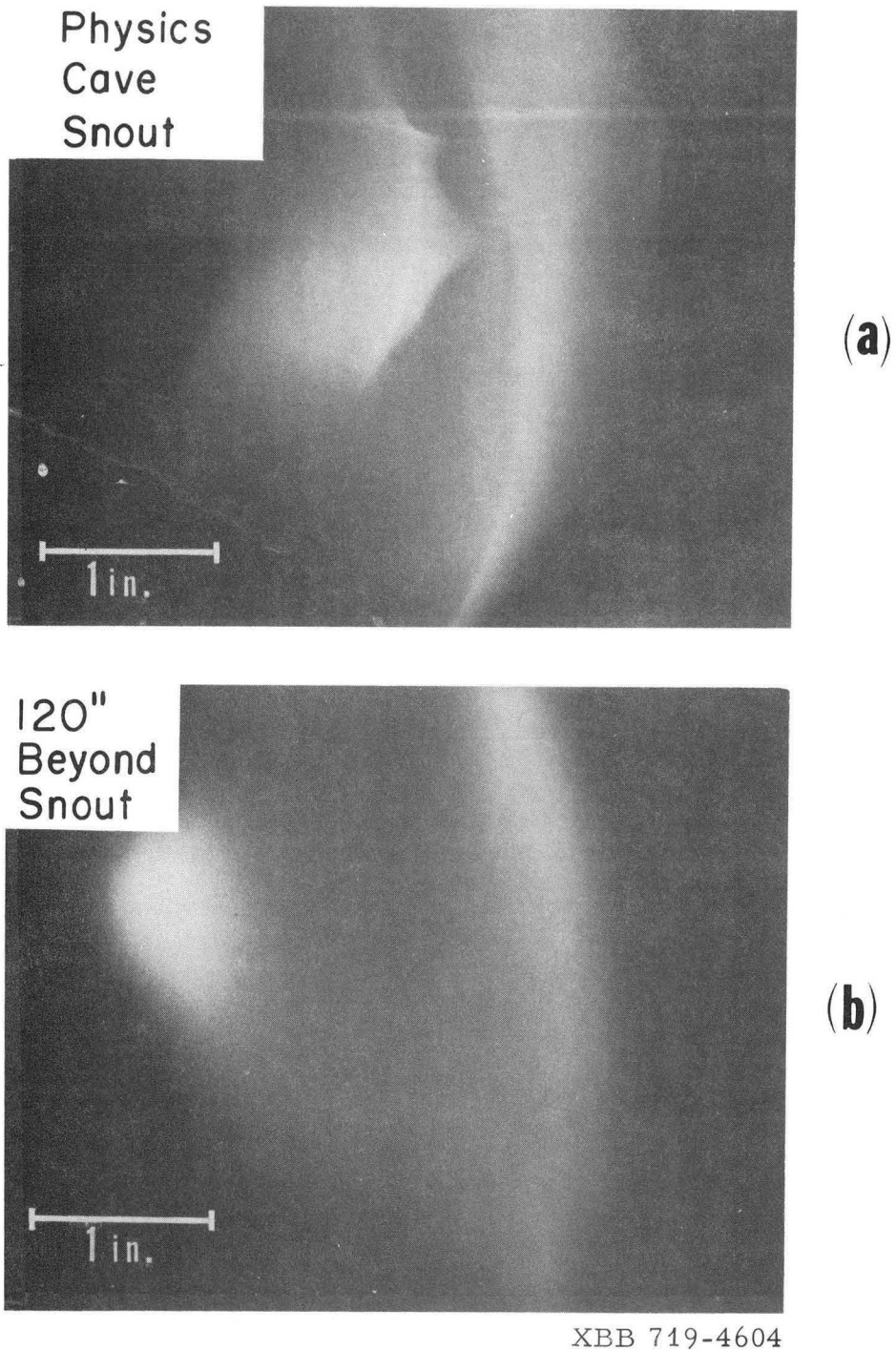
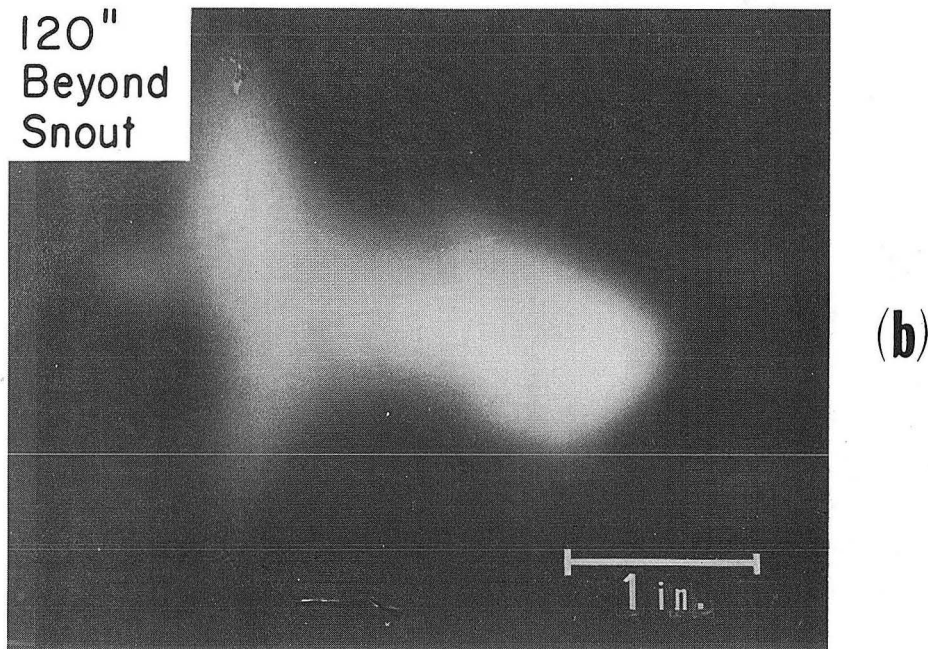
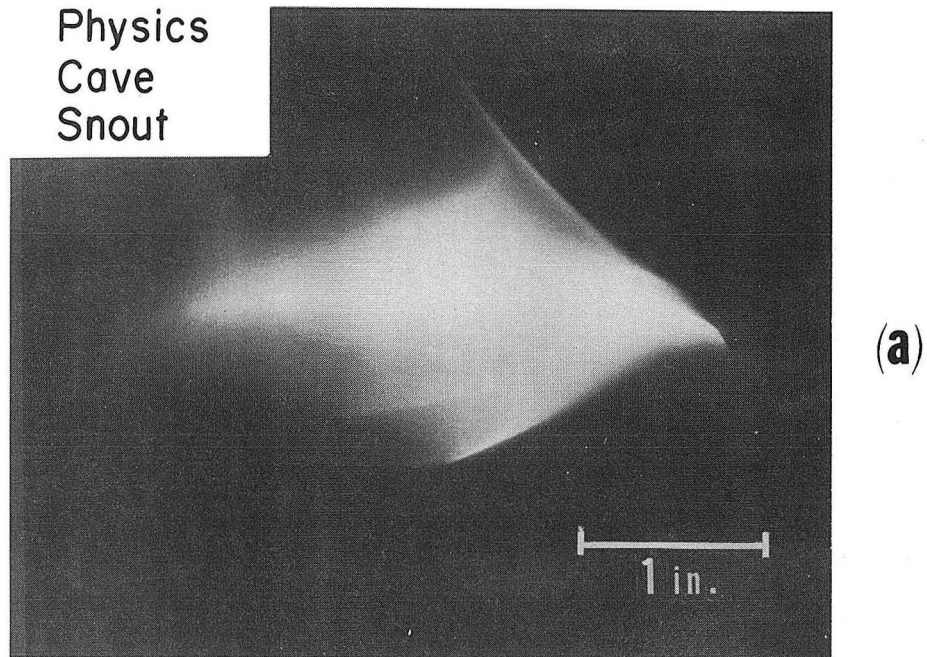


Fig. 14. (a) Beam photograph #9 at physics cave snout. (b) Beam 120" beyond snout. Both photographs are viewed looking in the direction of beam travel, main beam on the left, satellite beam on the right. The steering magnet was set to 281.5 mV; quadrupoles were set to 23.23 mV and 29.25 mV.



XBB 719-4599

Fig. 15. (a) Beam photograph #10 at physics cave snout.
(b) Beam 120" beyond snout. Both photographs are viewed looking in the direction of beam travel, main beam on the left, satellite beam on the right. The steering magnet was set to 281.5 mV; quadrupoles were set to 28.25 mV and 31.47 mV.

184 INCH CYCLOTRON BEAM LINE, 105 DEGREE PROBE LINE TO P.C. SNOOT

0									
22.000000	0.	0.	0.	0.	0.	1.000000	-0.		
27.000000	.470000	-7.500000	0.	9.900000	-0.	-0.	-0.		
22.000000	.470000	-10.000000	0.	-9.900000	-0.	-0.	-0.		
22.000000	.250000	-2.500000	.062500	8.000000	-0.	-0.	-0.		
22.000000	0.	2.500000	.100000	0.	-0.	-0.	-0.		
22.000000	.250000	-7.500000	-.100000	0.	-0.	-0.	-0.		
22.000000	-.470000	7.500000	0.	-9.900000	-0.	-0.	-0.		
22.000000	-.470000	10.000000	0.	9.900000	-0.	-0.	-0.		
22.000000	-.250000	2.500000	-.062500	-8.000000	-0.	-0.	-0.		
22.000000	0.	-2.500000	-.100000	0.	-0.	-0.	-0.		
22.000000	-.250000	7.500000	.100000	0.	-0.	-0.	-0.		
22.000000	0.	0.	0.	0.	0.	-1.000000	-0.		
22.000000	0.	2.500000	.200000	0.	-0.	-0.	-0.		
22.000000	0.	-2.500000	-.200000	0.	-0.	-0.	-0.		
22.000000	-.250000	-2.500000	-.300000	-15.000000	-0.	-0.	-0.		
22.000000	-.250000	2.500000	-.300000	15.000000	-0.	-0.	-0.		
22.000000	.300000	-5.000000	.400000	-15.000000	-0.	-0.	-0.		
22.000000	-.300000	5.000000	-.400000	15.000000	-0.	-0.	-0.		
22.000000	-.150000	5.000000	.300000	-15.000000	-0.	-0.	-0.		
22.000000	.150000	-5.000000	-.300000	15.000000	-0.	-0.	-0.		
22.000000	.250000	-6.250000	-.400000	15.000000	-0.	-0.	-0.		
22.000000	-.250000	6.250000	.400000	-15.000000	-0.	-0.	-0.		
22.000000	.750000	-11.000000	-0.	-0.	-0.	-0.	-0.		
12.000000	.300000	6.000000	.400000	16.000000	0.	0.	1.379400		
12.000000	-.900000	0.	0.	0.	0.	-.900000	-0.		
0.	0.	0.	-0.	-0.	-0.	-0.	-0.		-0.
7.000000	.750000	-11.000000	-0.	-0.	-0.	-0.	-0.		
24.000000	1234.000000	-0.	-0.	-0.	-0.	-0.	-0.		
13.000000	2.000000								
24.000000	0.	6.000000	6.000000	0.	1.000000	6.000000			
24.000000	1.000000	1.000000	1000.000000	1.000000	1000.000000	-0.			
16.000000	6.000000	142.800000							
6.000000	2.000000	5.500000	3.000000						
14.000000	3.539000	.158150	0.	0.	0.	.785730	1.000000		
14.000000	29.778800	1.613350	0.	0.	0.	10.770740	2.000000		
14.000000	0.	0.	-2.196870	.093920	0.	0.	3.000000		
14.000000	0.	0.	-13.989200	.142850	0.	0.	4.000000		
13.000000	1.000000								
3.000000	58.000000								
6.000000	4.000000	5.000000	5.000000						
13.000000	4.000000								
13.000000	1.000000								
24.000000	1234.000000	-0.	-0.	-0.	-0.	-0.	-0.		
3.000000	24.000000								
16.000000	5.000000	3.000000							
6.000000	2.000000	5.500000	3.000000						
6.000000	0.	1.000000	-0.						
4.000000	26.000000	-11.000000	0.						
4.000000	26.000000	-11.000000	0.						
2.000000	-14.000000	-0.							
13.000000	1.000000								
13.000000	4.000000								
3.000000	38.000000								
13.000000	1.000000								
13.000000	4.000000								
6.000000	0.	1.000000	-0.						
5.000000	20.000000	-4.752000	4.000000						
3.000000	6.000000								
5.000000	20.000000	5.702000	4.000000						
8.000000	-1.000000	0.	0.	0.	0.	0.	101.000000		
13.000000	1.000000								
13.000000	4.000000								
3.000000	100.000000								
3.000000	50.000000								
3.000000	56.000000								
6.000000	4.000000	5.000000	5.000000						
13.000000	1.000000								
13.000000	27.000000								
13.000000	4.000000								
24.000000	1234.000000	-0.	-0.	-0.	-0.	-0.	-0.		
3.000000	60.000000								
3.000000	60.000000								
6.000000	4.000000	5.000000	5.000000						
13.000000	1.000000								
13.000000	4.000000								
24.000000	1234.000000	-0.	-0.	-0.	-0.	-0.	-0.		
3.000000	50.000000								
73.000000	-0.								

XBL 719-1393

Fig. 16. Input data for "transport," describing the 184-inch cyclotron main beam by vectors, and the satellite beam as a six dimensional ellipsoid. The beam line extends from the 105 degree probe line to 120 inches beyond the physics cave snout.

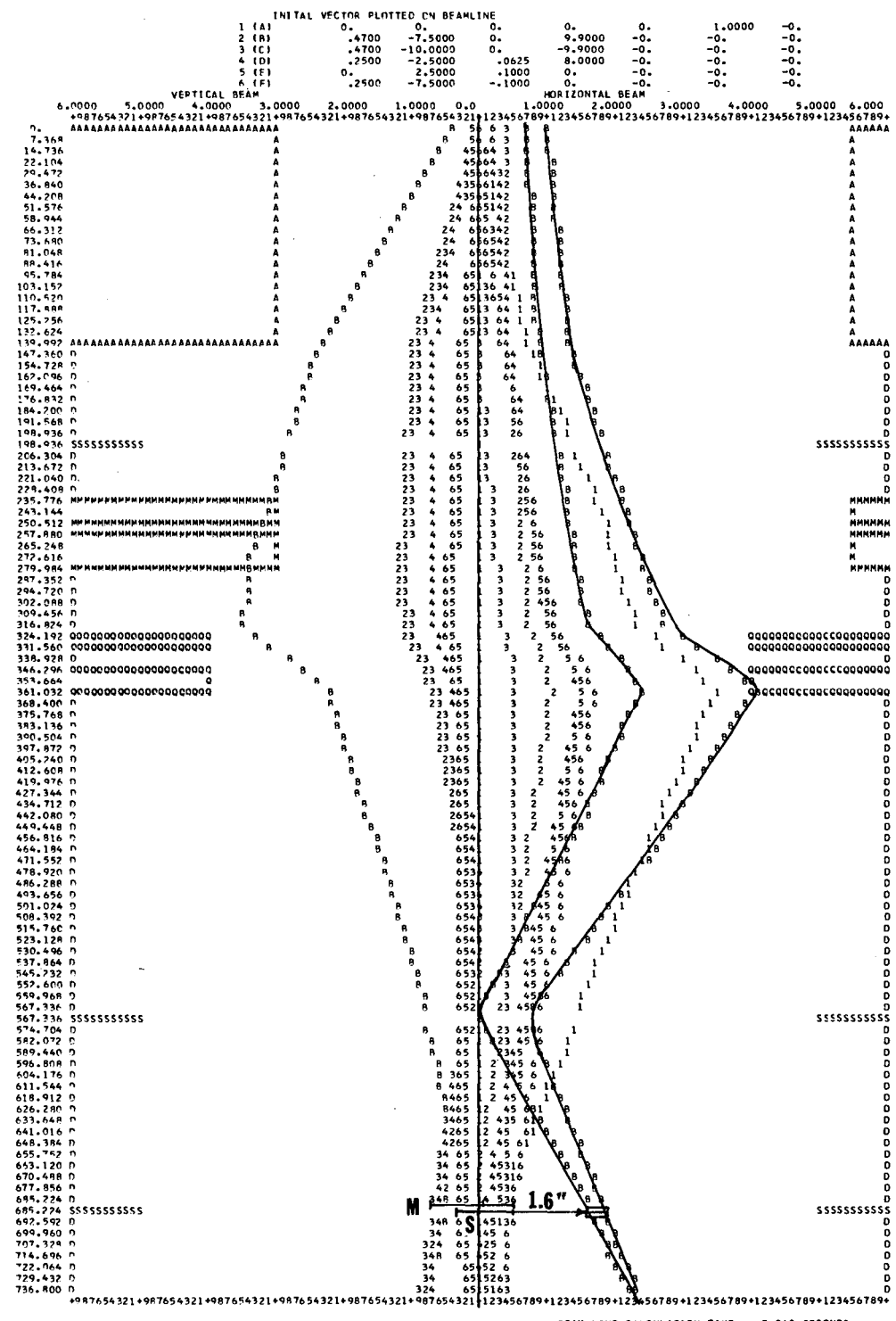


Fig. 18. Transport beam line, showing the main and satellite beams. Measured data corresponding to quadrupole settings of photo 3 (Fig. 3).

LEGAL NOTICE

This report was prepared as an account of work sponsored by the United States Government. Neither the United States nor the United States Atomic Energy Commission, nor any of their employees, nor any of their contractors, subcontractors, or their employees, makes any warranty, express or implied, or assumes any legal liability or responsibility for the accuracy, completeness or usefulness of any information, apparatus, product or process disclosed, or represents that its use would not infringe privately owned rights.

TECHNICAL INFORMATION DIVISION
LAWRENCE BERKELEY LABORATORY
UNIVERSITY OF CALIFORNIA
BERKELEY, CALIFORNIA 94720